

AD-A117 033

FORD MOTOR CO DEARBORN MICH F/8 11/4  
CERAMIC LIFE PREDICTION METHODOLOGY - HOT SPIN DISC LIFE PROGRA--ETC(U)  
APR 82 R R BAKER, L R SWANK, J C CAVERLY DAA646-77-C-0028  
AMMRC-TR-82-26 NL

UNCLASSIFIED

1981

1981

1981

1981

1981

1981

1981

1981

1981

1981

1981

1981

1981

1981

1981

1981

1981

1981

1981

1981

1981

1981

1981

1981

1981

1981

1981

1981

1981

1981

1981

1981

1981

1981

1981

1981

1981

1981

1981

1981

1981

1981

1981

1981

1981

1981

1981

1981

1981

1981

1981

1981

1981

1981

1981

1981

END  
DATE  
FILMED  
8-82  
DTIC

AD A117033

12



AD

AMMRC TR 82-26

CERAMIC LIFE PREDICTION METHODOLOGY -  
HOT SPIN DISC LIFE PROGRAM

April 1982

R. R. BAKER, L. R. SWANK and J. C. CAVERLY  
Ford Motor Company  
P.O. Box 2053  
Dearborn, Michigan 48121

INTERIM REPORT

Contract No. DAAG46-77-C-0028

Approved for public release; distribution unlimited.

DTIC  
JUL 19 1982  
H

DTIC FILE COPY

Prepared for

ARMY MATERIALS AND MECHANICS RESEARCH CENTER  
Watertown, Massachusetts 02172

82 07 19 085

The findings in this report are not to be construed as an official Department of the Army position, unless so designated by other authorized documents.

*Mention of any trade names or manufacturers in this report shall not be construed as advertising nor as an official indorsement or approval of such products or companies by the United States Government.*

**DISPOSITION INSTRUCTIONS**

*Destroy this report when it is no longer needed.  
Do not return it to the originator.*



**UNCLASSIFIED**

**SECURITY CLASSIFICATION OF THIS PAGE(When Data Entered)**

**Block No. 20**

**ABSTRACT**

A rotating disc was designed to fail due to time dependent mechanisms. Several discs were fabricated and a previously existing test rig was developed to test the discs at the design conditions. A successful calibration test was conducted at the design conditions of 2300°F rim temperature and 50,000 rpm. The disc failed after eight and one-half hours of steady state testing indicating that the design was successful, since the failure was due to a time dependent mechanism.

**UNCLASSIFIED**

**SECURITY CLASSIFICATION OF THIS PAGE(When Data Entered)**

## FORWARD

This report presents the complete work done during the period of October 1, 1979, through December 31, 1980, on the Hot Spin Disc Life Program, which is a part of the "Methodology for Ceramic Life Prediction Program," initiated by Dr. Robert Schulz of the Office of Conservation, Division of Transportation Systems, Department of Energy, and monitored by the Army Materials and Mechanics Research Center under Contract Number DAAG-46-77-C-0028. Funds for this phase of the work were provided by AMMRC. This work was necessary in formulating a methodology for ceramic life prediction so that ceramic materials can be used in high temperature structural applications. The principal investigator of this program was R. R. Baker, Ceramic Materials Department, Engineering and Research staff, Ford Motor Company. The technical monitor was Dr. E. M. Lenoë of AMMRC. The authors wish to thank Drs. E. M. Lenoë and R. H. Katz of AMMRC for suggestions in carrying out the program, and Mr. A. F. McLean, Manager, Ceramic Materials Department, Ford Motor Company, for careful reading and constructive criticism of the report.



Accession For	
NTIS GRA&I	<input checked="" type="checkbox"/>
DTIC TAB	<input type="checkbox"/>
Unannounced	<input type="checkbox"/>
Justification	<input type="checkbox"/>
By _____	
Distribution/	
Availability Codes	
Dist. Statement or	
Dist. Approval	
A	

## TABLE OF CONTENTS

	<u>Page</u>
Forward . . . . .	i
1. Introduction . . . . .	1
2. Design of Disc . . . . .	2
3. Disc Machining . . . . .	11
4. Rig Development . . . . .	15
5. Initial Calibration Test . . . . .	17
6. Summary . . . . .	20
7. Recommendations . . . . .	20
8. References . . . . .	21
9. Appendix A Calculation of Constant "B" . . . . .	24
10. Appendix B Nomenclature . . . . .	27
11. Appendix C Simplification of Reliability Versus Time Formula . . . . .	28
12.. Table I - Thermal Properties . . . . .	30
13. Table II - Elastic Properties . . . . .	31
14. Table III - Crack Velocity Parameters . . . . .	32
15. Table IV - Critical Stress Intensity Factor . . . . .	33
16. Table V - Stress Rate Data of Norton NC-132 HPSN . . . . .	34

## INTRODUCTION

Since the early sixties there has been considerable interest in silicon nitride as an engineering material. Sage and Histed<sup>(1)</sup> reviewed some of the applications for silicon nitride and suggested the use of silicon nitride in gas turbines. An increase of 100°C in turbine stator blade temperature was forecast. Glenn and Taylor<sup>(2)</sup> reviewed the material properties of silicon nitrides and noted the high strength at elevated temperatures of silicon nitride. Evans and Wiederhorn<sup>(3)</sup> observed the phenomenon of static fatigue in hot pressed silicon nitride, and noted that this presented a design problem in the application of the material in highly stressed applications at elevated temperatures.

The phenomenon of static fatigue is well known in metals where it may be caused by slow crack growth. Siverns and Price<sup>(4)</sup> observed that the crack growth rate in steel at elevated temperatures was correlated with the power law relationship

$$V = AK_I^n \quad (1)$$

Evans and Johnson<sup>(5)</sup> suggested that this equation could be applied to ceramics and that the cause of slow crack growth was grain boundary sliding. This is due to the glassy phases in the grain boundary softening at elevated temperature and allowing the crystalline grains of silicon nitride to slide relative to one another at the tip of the crack where the stresses are the highest. The sliding of the grains causes the crack to grow and continued application of stress and temperature could cause catastrophic failure<sup>(6)</sup>.

Williams and Evans<sup>(7)</sup> proposed the double torsion test to measure the values of the crack velocity exponent, and the premultiplier in Eqn. 1. The double torsion test is a simple test in concept that loads a pre-cracked specimen in a manner that the stress intensity factor remains constant as the crack grows. This simplifies the analysis and makes it possible to determine A and n from the load versus time curve.

Charles<sup>(8)</sup> proposed stress rate testing to determine the crack velocity exponent and demonstrated its use on glass. In stress rate testing MOR bars are

fractured at two different stress rates to obtain two pairs of data - the fast fracture stress and its corresponding stress rate. From the pairs of data the slow crack growth parameters are calculated.

Several experimenters have conducted stress rupture tests on ceramic materials. Trantina<sup>(9)</sup> conducted stress rupture tests on Norton's NC-132 material, a hot pressed silicon nitride. His tests were conducted in three-point bending on bars of 0.9 inch span with a cross section of 0.1 inch x 0.1 inch. Quinn<sup>(10)</sup> conducted stress rupture tests on several different structural ceramic materials. His tests were conducted in four-point bending on a fixture with a 1.5 inch outer span, a 0.75 inch inner span, and a bar with a 0.110 inch base and a 0.085 inch height.

Previous experimenters conducted their tests on small parts with very small volumes compared to the volume of typical gas turbine components. Previous tests were also conducted at uniform temperatures, but gas turbine components have large temperature gradients. This suggested the need for generating a time to failure database on a component the size of a typical gas turbine component with temperature and stress distributions similar to gas turbine components. This database could then be used as a test case for evaluation of models of failure and computer programs used to predict time to failure.

The hot spin rig shown in Fig. 1 has accumulated many hours of testing ceramic gas turbine rotors at elevated temperatures and at angular speeds equal to gas turbine speeds. The rig proved very reliable under these conditions, therefore, it was selected to conduct the tests required. Operation and details of the rig have been previously described<sup>(11)</sup>. A rotating disc was designed to fail due to time dependent mechanism utilizing available techniques and models. The rig was developed to conduct the tests, and an initial calibration test was conducted.

## II. DESIGN OF DISK

The finite element grid of the rotating components used to calculate the temperature distribution in the spin disc is shown in Fig. 2. The physical parts

represented by the finite elements are shaded and labeled for identification. The finite elements that compose the model are rectangular or triangular in shape. The material thermal properties used in the analysis are given in Table I.

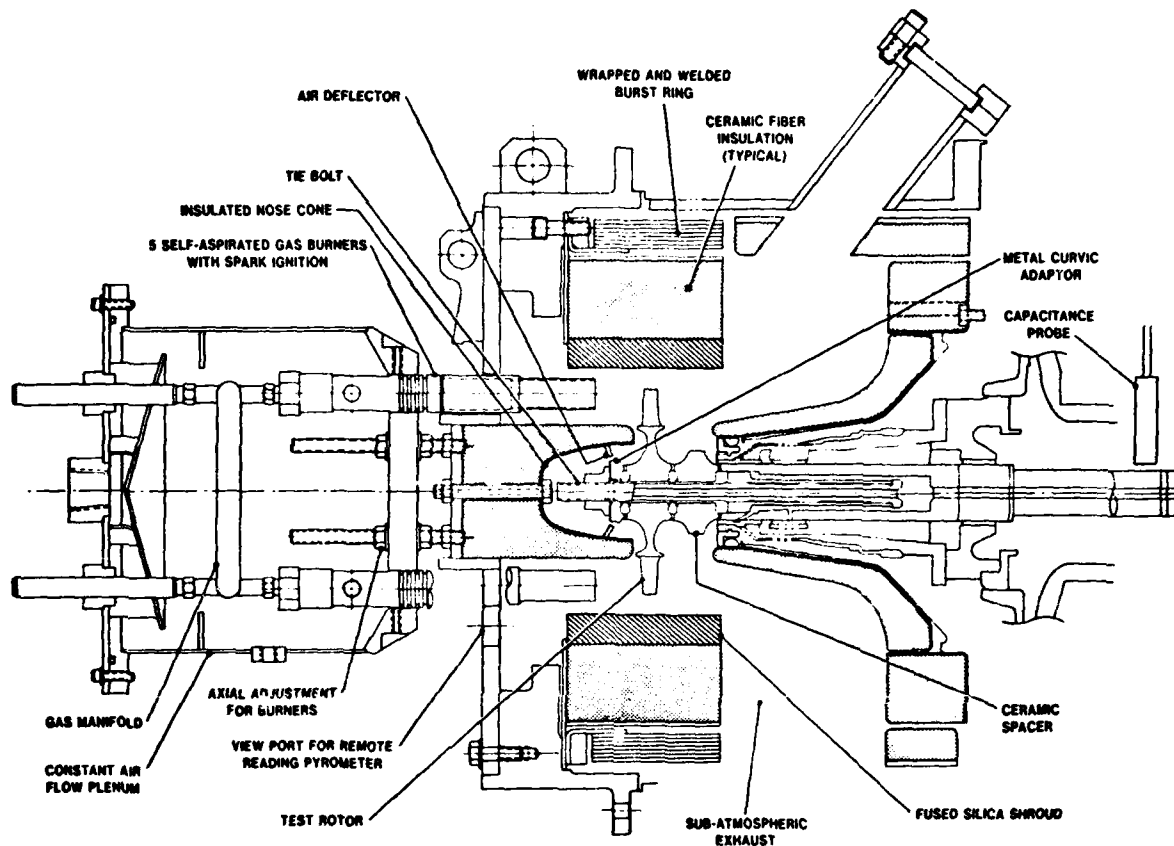


Figure 1-Hot spin test rig.

The temperatures within the rotating components were determined by these boundary conditions and the thermal conductivities of parts in the assembly. Heat was applied to the front face and rim of the spin disc with propane gas burners. The temperature of the front face was measured with a radiation pyrometer and the measured temperatures were used as input to the analysis. The tie bolt was cooled with air as shown on Fig. 2. The cooling air mass flow rate and associated heat transfer coefficients formed the boundary conditions. A portion of the tie bolt cooling air was directed to the metal curvic adaptor for cooling and the mass flow rate and heat transfer coefficients formed the boundary conditions for the exterior of the tie bolt, nut, and metal

curvic adaptor. The downstream side of the spin disc and the exterior of the ceramic curvic spacer were heated with hot gases and air swirling in the rig, thus forming another boundary condition. The labyrinth and bearing region on the shaft form the last boundary condition. As part of the model, radiation heat transfer was included between the spin disc bore, ceramic curvic spacer bore and the tie bolt.

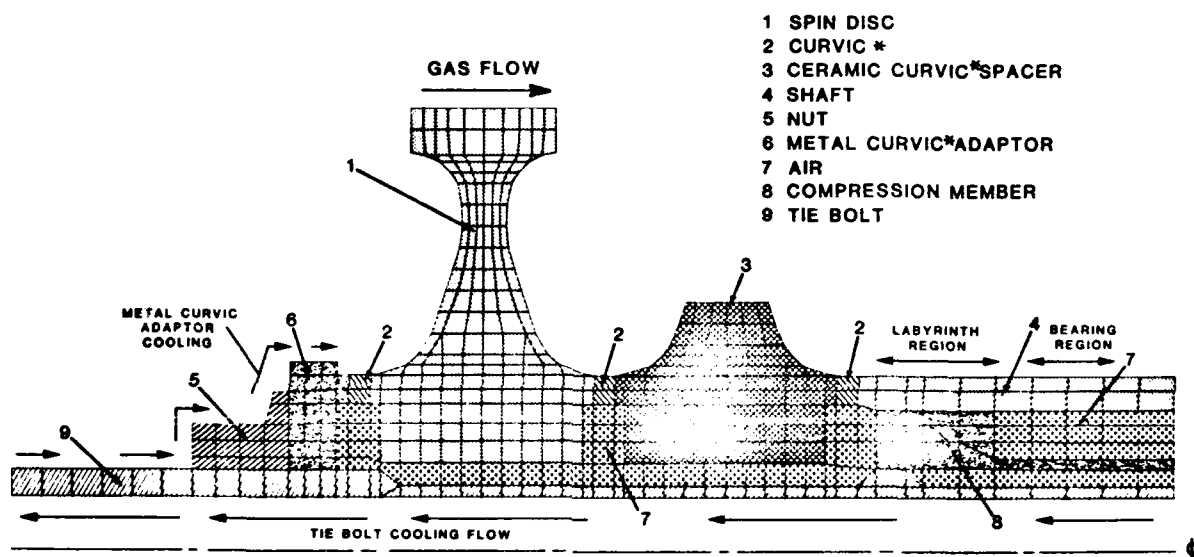


Figure 2-Rotating components heat transfer model.

Calculated temperature distributions were compared to results from temperature sensitive paints and adjustments to the model were made to obtain agreement. Temperature measurements of the air in the cooling streams were also used as input to the model and as a check on the validity of the model; for example the temperature of the tie bolt cooling air was measured as it entered the labyrinth and as it left the tie bolt. The temperature of the air in the labyrinth region was used as input to the model and the air exit temperature was compared to the calculated value as a check on the model.

Figure 3 illustrates the finite element grid used to calculate the stresses in the spin disc. The temperature distribution was derived from the heat transfer model and transferred to the stress finite element grid. The temperature contour plot at the test design conditions is illustrated in Fig. 4. The combined thermal and centrifugal stresses, at this test condition, are illustrated in Figs. 5 through 9. These stress plots show the maximum principal tensile stress, the tangential stress, the radial stress, the axial stress, and the maximum shear stress. The elastic properties used in the stress calculations are given in Table II.

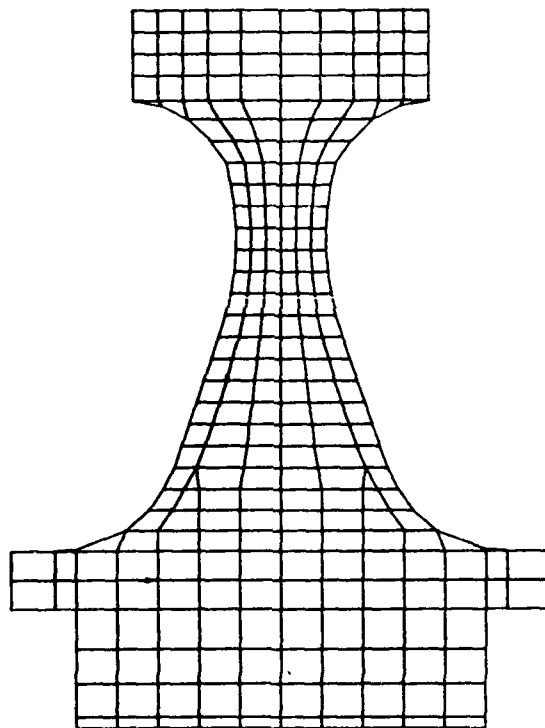


Figure 3- Disc finite element grid.

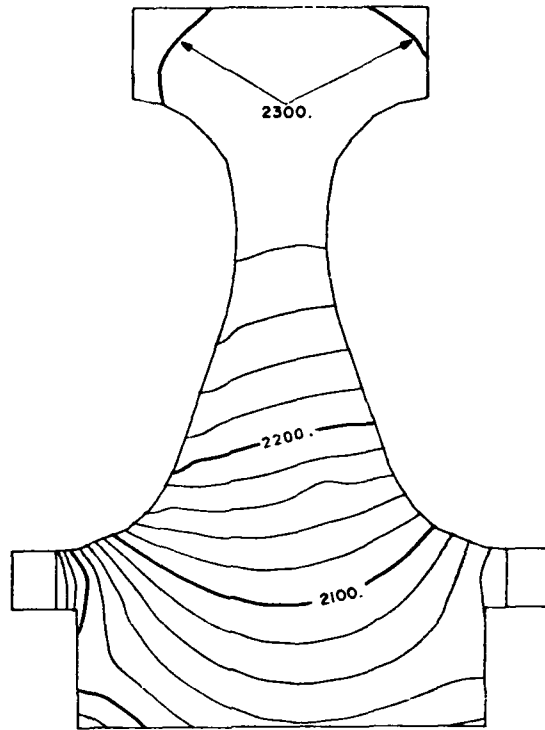


Figure 4 - Isotherms [°F] in disc at 50,000 rpm.

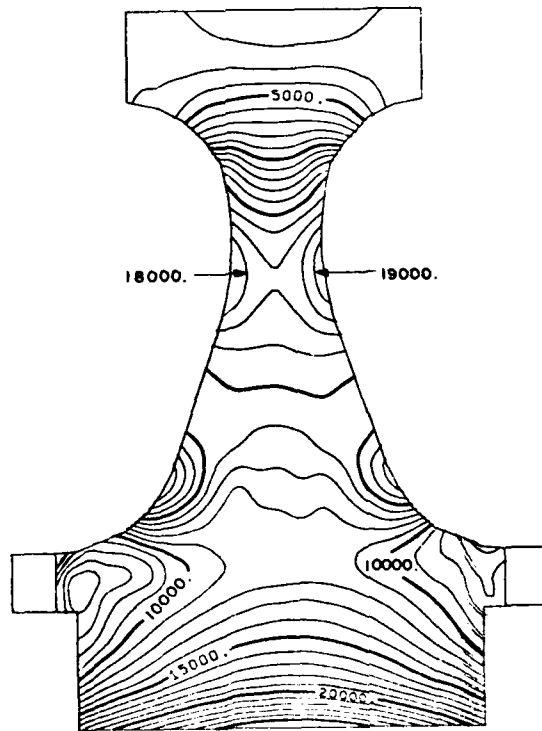


Figure 5 - Maximum principal stresses [psi] in disc combining thermal and centrifugal stresses at 50,000 rpm.

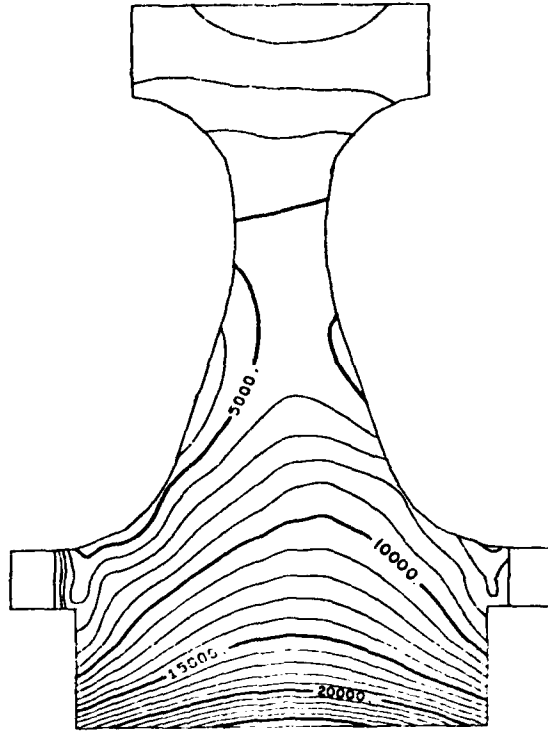


Figure 6 - Tangential stresses [ psi ] in disc combining thermal and centrifugal stresses at 50,000 rpm.

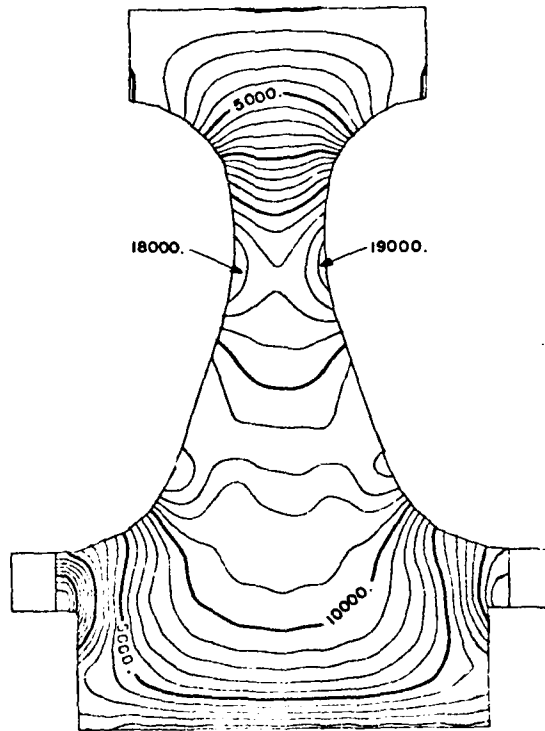


Figure 7 - Radial stresses [ psi ] in disc combining thermal and centrifugal stresses at 50,000 rpm.

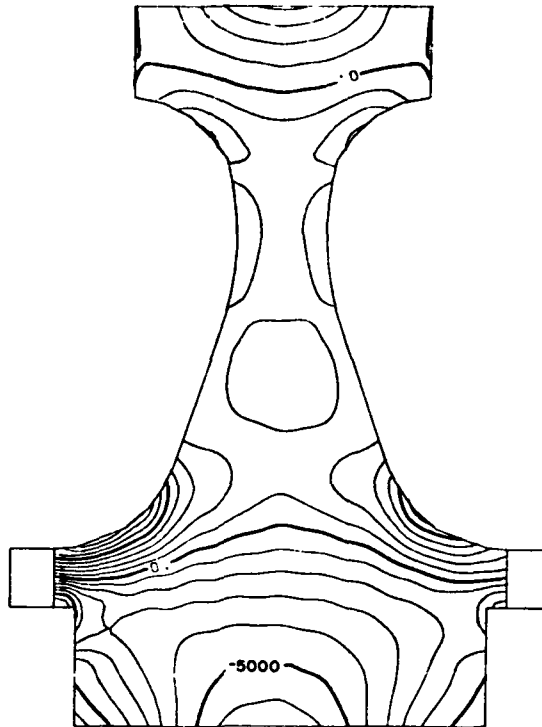


Figure 8 - Axial stresses [psi] in disc combining thermal and centrifugal stresses at 50,000 rpm.

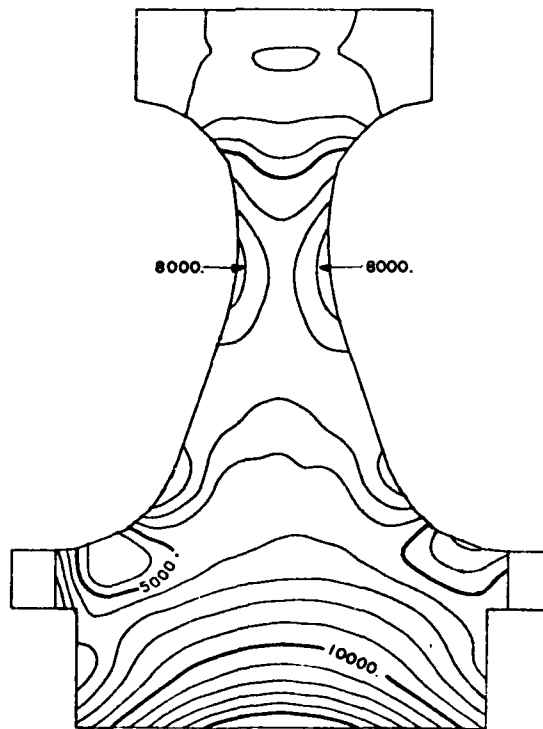


Figure 9 - Maximum shear stresses [psi] in disc combining thermal and centrifugal stresses at 50,000 rpm.

The reliability versus time formula <sup>(12)</sup> used in this report is shown in Eqn. (1). Definition of the symbols is given in appendix B.

$$R = \exp - \left[ \left[ \left( \ln \frac{1}{R_{ff}} \right)^{\frac{n-2}{m}} + \frac{\sigma_t^n}{\sigma_B^{n-2}} \right]^{\frac{m}{n-2}} \right] \quad (1)$$

During this work, Eqn. 1 was reduced to a simpler form shown as Eqn. 2. The detailed algebraic steps are given in Appendix C.

$$R = R_{ff} \left( 1 + \frac{\sigma_t^2}{B} \right)^{\frac{m}{n-2}} \quad (2)$$

Equation 2 is much simpler for computation and was programmed for digital computer use to calculate time-dependent reliabilities for steady state temperature and loading conditions. The equation was evaluated for each element of the finite element grid of Fig. 3 based on the maximum principal stress, the Weibull modulus, the crack velocity exponent, the value of B, and the fast fracture reliability of the element. The Weibull modulus, crack velocity exponent, and the value of B were linearly interpolated from a table of these parameters versus temperatures, based on the centroidal temperature of the element.

Equation 2 shows that when time equals zero the time dependent reliability is simply the fast fracture reliability. The fast fracture reliability was evaluated by integrating the normal stress around the unit sphere in each finite element and evaluating the Weibull integral for each element <sup>(13,14)</sup>.

Two data bases, double torsion data and stress rate data, were available for the calculation of time dependent reliabilities. Both data bases yield the two parameters "B" and "n" essential for the evaluation of Eqn. 2. Figure 10 shows the calculation flow path utilizing double torsion data. Fast fracture testing produced a collection of fast fracture data which was analyzed using maximum likelihood estimation methods <sup>(15)</sup> to determine the characteristic modulus of rupture and the Weibull modulus. The stress distributions along with the Weibull parameters were input to a computer program which evaluated Weibull's formula for fast fracture reliability, which in turn was input to another computer program which calculated time dependent reliability. From

double torsion testing the crack velocity exponent, the pre-multiplier "A", and the critical stress intensity factor were obtained. With these parameters and the value of the stress intensity factor coefficient, "Y", the value of "B" was calculated<sup>(12)</sup>. The value of "B" and crack velocity exponent "n" were input to a computer program that evaluated the reliability versus time.

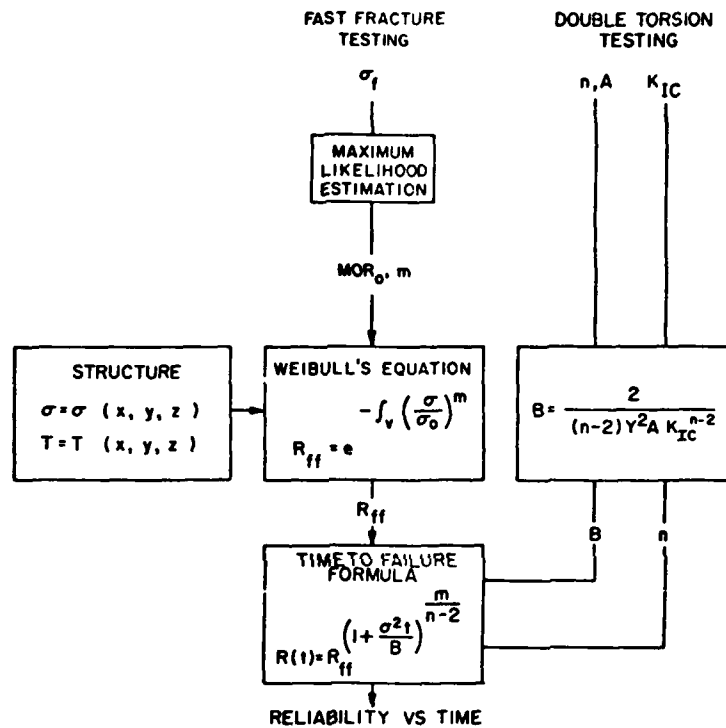


Figure 10 - Calculation flow path utilizing double torsion data

Figure 11 shows the calculation flow path utilizing stress rate testing data to obtain reliability versus time. Stress rate testing determined pairs of fast fracture strength and the corresponding value of stress rate. The value of "B" and the crack velocity exponent "n" were calculated from the pairs of strength and stress rate with the formulas shown on the figure<sup>(16)</sup>. The fast fracture calculation was the same as that used with double torsion data.

The calculation procedures shown in Figs. 10 and 11 were used to design the disc. The design was arrived at by checking trial designs with the reliability

versus time calculation procedures until a satisfactory design was obtained. The reliability versus time results are shown on Fig. 12. Note that the two data bases, double torsion and stress rate, give widely different results.

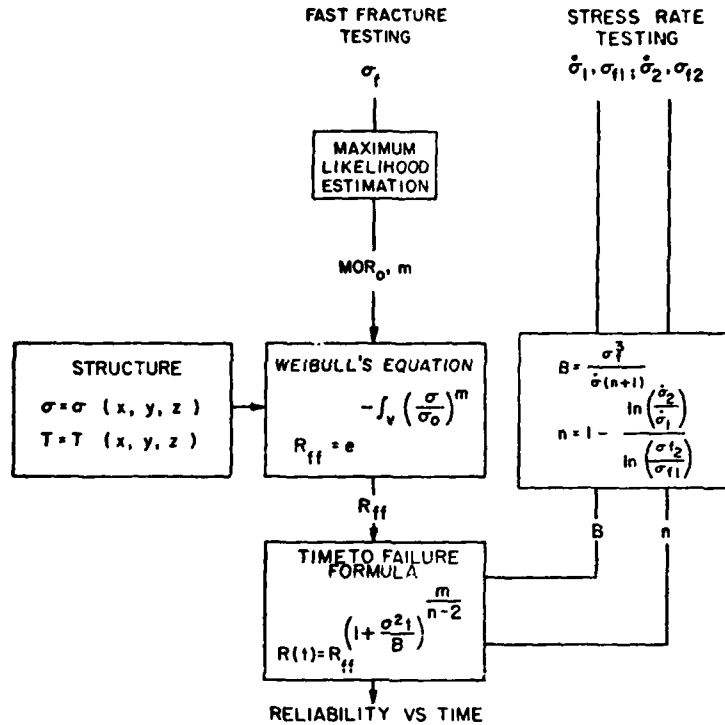


Figure 11 - Calculation flow path utilizing stress rate data

### III. DISC MACHINING

Life prediction discs were machined from six inch square, one and three-eighths inch thick billets of hot pressed silicon nitride (NC132).\* The four inch diameter discs were made in several steps beginning with a slicing operation in which an octagonal block was cut out of each billet. This piece was ground to the approximate thickness of the finished disc and a center hole or bore was then core drilled through with a diamond core drill. The bore was then ground

\* Certified Billets from Norton Company

to finish size allowing the disc to be centrally mounted for further grinding operations. Most of the grinding was done on a Brown and Sharp Universal grinder. Initial material removal was accomplished using 120-150 grit diamond plate and a commercial water soluble coolant (X50-2 Chem-trend). Final dimensions were produced with 200-250 grit wheels.

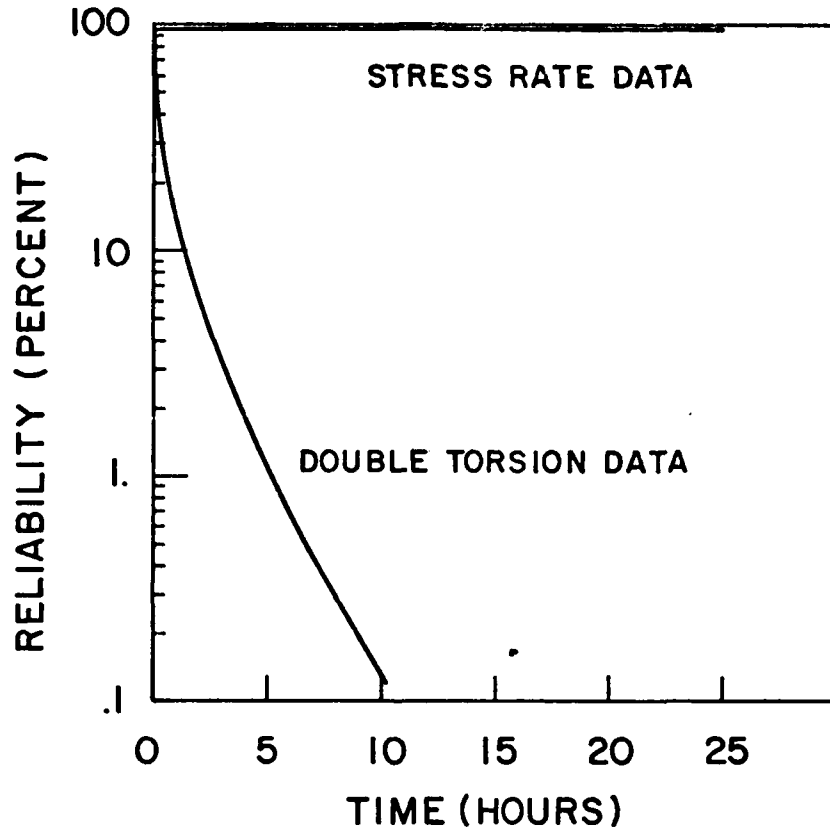


Figure 12 - Calculated reliability versus time

The disc face contours were produced by specially shaped contour grinding wheels shown in Fig. 13. These wheels were rotated at 12-13000 rpm and were fed into the disc side as shown in Fig. 14 in a three step operation. The disc was rotated at 100 rpm in the opposite direction to the grinding wheel rotation. This allowed control of the grinding and stability of the set-up.

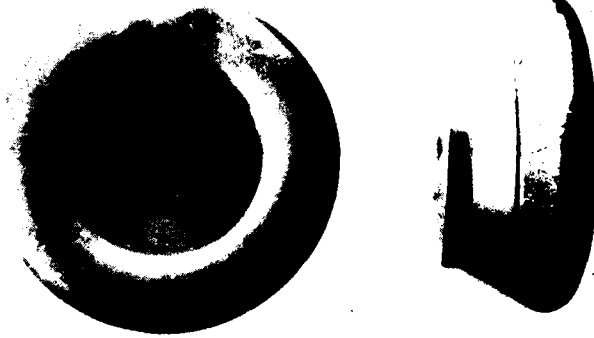


Figure 13 - Contour grinding wheel

**3 STEP PROCEDURE FOR DISC CONTOURING**

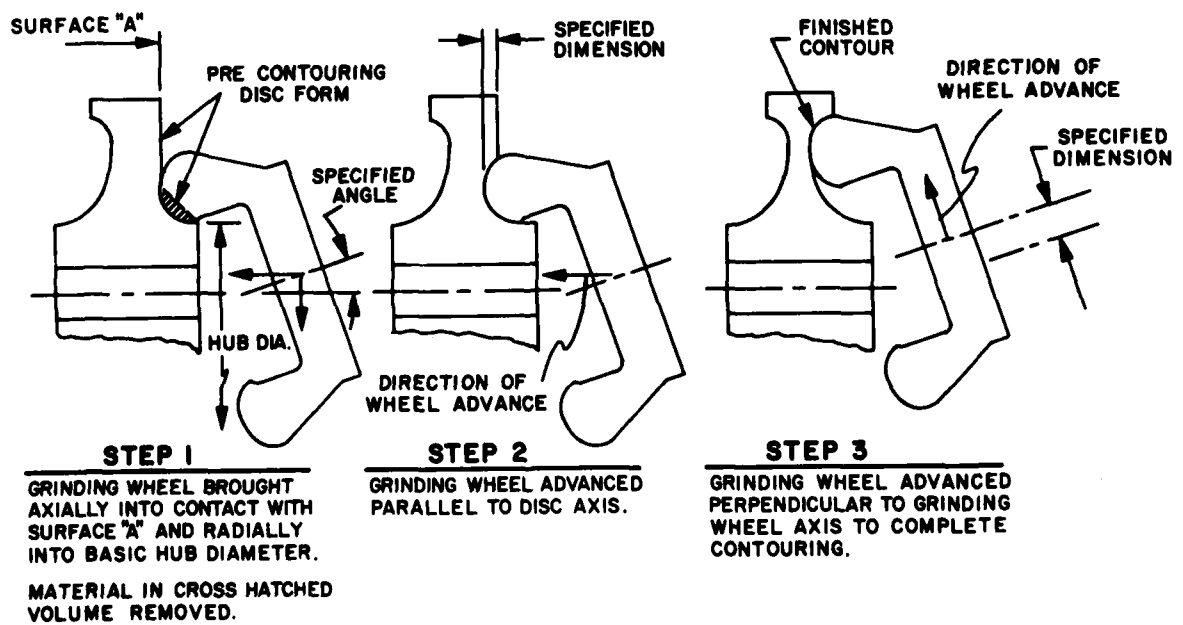


Figure 14 - Procedure for disc contouring

All grinding tools, including contour wheels, were diamond coated and final polishing of the disc contours was done with diamond pastes on a brass lap. The lap was in the form of a ball on a 1/4" diameter shank and the lap was driven by a hand held electric drill. The disc was slowly rotated on an arbor and the contour was polished to a 1-2 $\mu$ inch finish by successively using diamond pastes of 30-40, 6-12 and 1-5 micron grit.

Finally the curvic couplings used to mount the disc to the shaft were ground by diamond coated grinding wheels on special purpose curvic grinding equipment. The discs were then zygoed for possible cracks caused by grinding and then dimensionally inspected. Figure 15 shows the completed disc ready for testing.



Figure 15 - Disc ready for testing

#### IV. RIG DEVELOPMENT

The hot spin rig was originally developed to conduct tests on bladed discs. Considerable experience had been obtained on bladed discs at a platform temperature of 1800°F<sup>(17)</sup>. In addition 25 hours of testing had been conducted at a platform temperature of 2000°F at a speed of 50,000 rpm<sup>(18)</sup>. Three hours of testing had been conducted at a platform temperature of 2200°F and speeds above 30,000 rpm. Since no direct experience on unbladed discs at the temperatures required for the Hot Spin Disc Life Program existed, a development program was necessary.

Tests on actual Life Prediction discs began in mid July of 1980, with the initial attempts to run disc NC1316 at 2300°F rim temperature. The original burner configuration with 5 straight burners was found to give a maximum rim temperature of 2130°F. A calibrated radiation pyrometer, Ircon model 300T5, was sighted through a hole in the rig wall to determine the actual disc temperature. A slight temperature dependence on speed was found but it was obvious that the original system would not produce the required 2300°F rim on an unbladed disc.

The first modification to the burner system was to increase the number of burners from 5 to 12. Tests with this set-up produced maximum rim temperatures of 2170°F.

Tests with individual burners showed that the gas flame temperature was running at 3100 to 3200°F; however, the burners were located such that only part of the gas flame touched the disc rim. The flames did not impinge directly onto the disc rim. It was decided to modify two burners so that the flame would impinge directly on a portion of the rim of the front face of the disc. These burners were cut and rewelded at an angle of 10° and the total number of burners was reduced to five. In addition, as shown in Fig. 16, the nose cone portion of the rig was redesigned and fabricated. The original design ducted the bolt cooling air, exhausted through the end of the bolt, back over the curvic adaptor and up the forward face of the disc. This 600°F air produced a veiling as well as a cooling effect. The redesigned parts ducted this cool exhaust air

out of the rig through a hole along the center of the nose cone exhausting to ambient. Also some of the rig insulation behind the disc, which ran at very high temperatures, was increased in area to increase the hot surfaces radiating heat to the rear face of the disc.

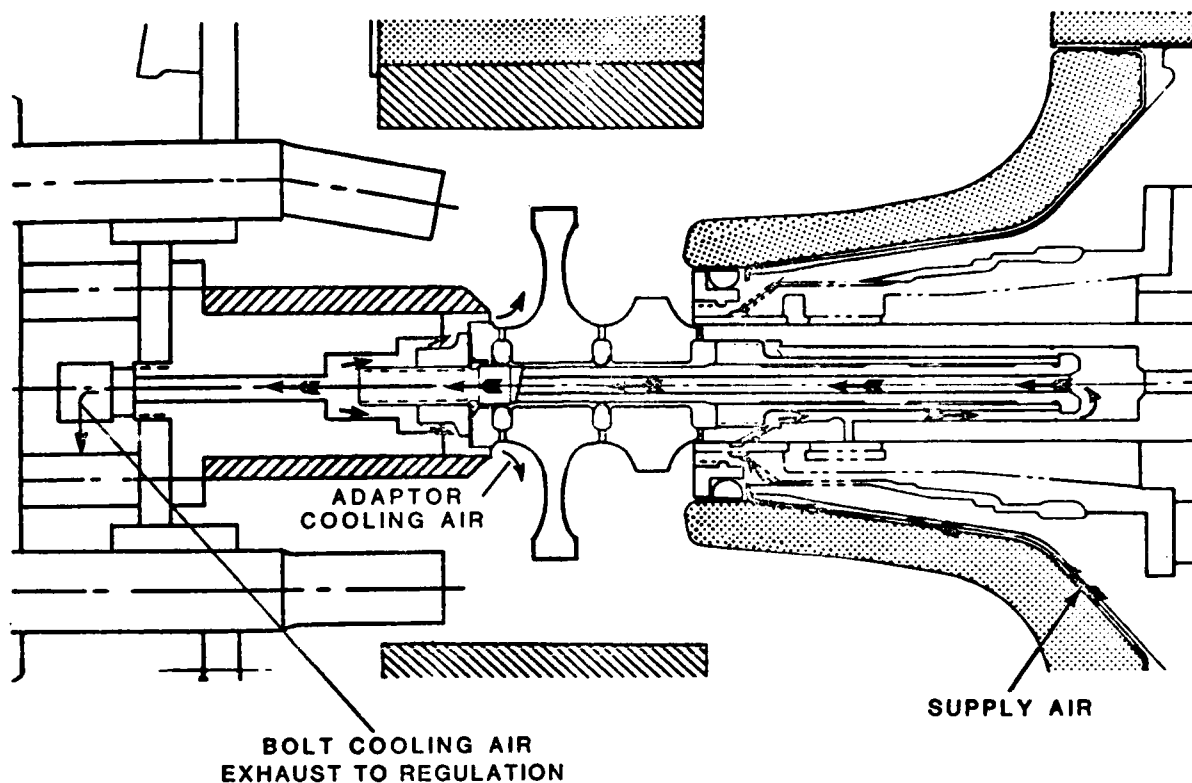


Figure 16 - Tie bolt cooling air distribution

This design was tested in mid October of 1980. The first tests were run without restricting the bolt exhaust air. A rim temperature of  $2370^{\circ}\text{F}$  was easily obtained; however, the jet effect of the bolt exhaust air drew hot gases down the disc face into the curvic area and overheated the curvic adaptor. This over-heating softened the adaptor and caused the rotor, NC1316, to fail at 24000 rpm. Apparatus was added externally to the rig to allow modulation of the bolt exhaust air. This caused some of the bolt cooling air to flow over the metal curvic adaptor maintaining it at an acceptable temperature. A thermocouple was installed in the adaptor cooling air flow stream to monitor the temperature.

These modifications completed the rig development. The details of the tie bolt cooling air distribution are shown in Fig. 16. This illustrates how the tie bolt cooling air is split so that a portion of the air flows over the metal curvic adaptor for cooling. The overall schematic of the final rig configuration is shown in Fig. 17. The modifications to the burner tubes, nose cone, and insulation may be seen by comparing Fig. 17 to Fig. 1.

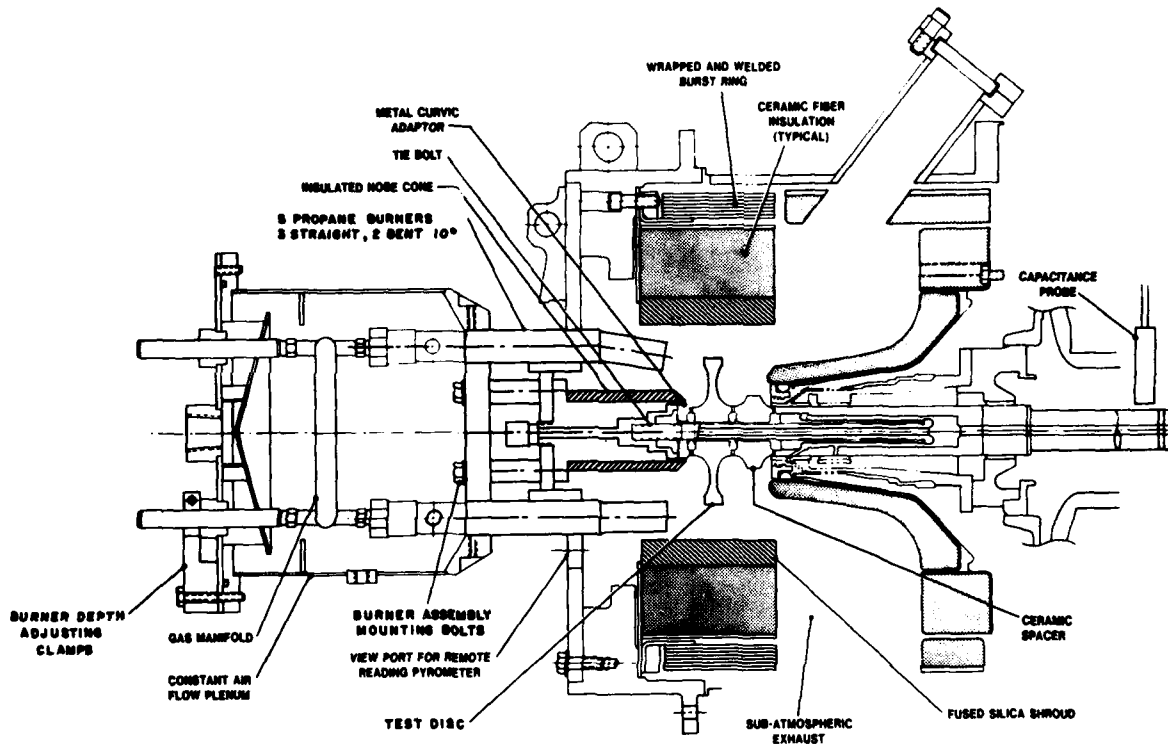


Figure 17 - Final rig configuration

## V. INITIAL CALIBRATION TEST

An initial calibration test was conducted on disc NC 1318 to verify the analytical calculations and to determine if failure would occur within a reasonable time frame. The rig configuration used is shown in Fig. 17. The steady state temperatures selected were the same as those shown in Fig. 4 with a corresponding speed of 50,000 rpm. The steady state conditions were arrived at by igniting the burners with the disc rotating at 2000 rpm. The disc was then

accelerated to 10,000 rpm. The speed and temperature were stabilized at 10,000 rpm. The disc was then accelerated to 24000 rpm, where the speed and temperature were stabilized. The temperature gradient was established at 24000 rpm so that the thermal stress distribution was established and the relative motion between rotating components would be minimized during the acceleration to 50,000 rpm. After the temperature gradient stabilized, the disc was slowly accelerated to 50,000 rpm. At 50,000 rpm the temperatures and air flows were stabilized and they remained constant for the rest of the test.

Failure occurred eight and one-half hours after reaching 50,000 rpm. No indications of problems occurred on any of the instrumentation used to monitor the test, which indicates that the test rig was performing properly. After the test, the rig was disassembled and the parts carefully examined to determine if failure occurred due to slow crack growth. The stress analysis indicated that the most severe combination of temperatures and stresses was in the neck region. Figure 18 is a photograph of the hub region after the test, showing that the hub remained intact. This shows that the failure did not initiate in the hub region. Figure 19 shows a piece of the neck region showing the fracture and a crack that developed parallel to the main fracture. Figure 20 shows this piece rotated so that the main fracture surface can be seen. It is believed that the pattern of this crack indicates slow crack growth occurring normal to the radial stress in the neck region. The conclusion was that the test procedure and conditions were developed to the point where discs could be tested to failure under conditions of slow crack growth.



Figure 18 - Hub region of the disc after the test

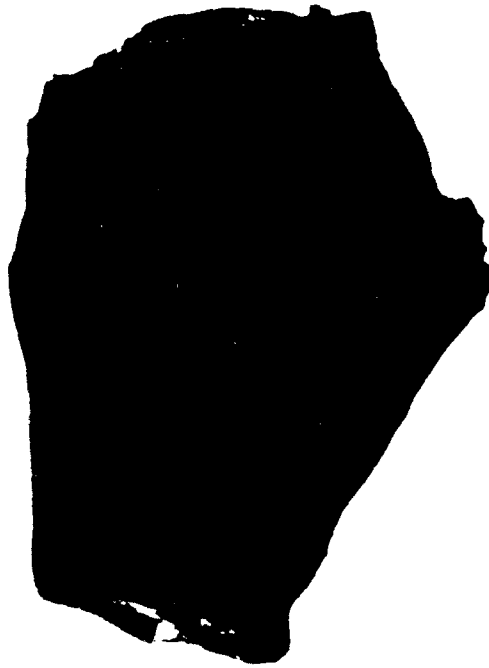


Figure 19 - View of the crack in the neck, normal to the machined surface



Figure 20 - View of the crack in the neck showing adjacent fracture surface

## VI. SUMMARY

A disc was designed to fail under the conditions of slow crack growth. Several discs were fabricated. The existing hot spin rig was modified and developed to test the disc under the design conditions. An initial calibration test was successfully conducted to verify the design.

The literature was searched for slow crack growth material properties required to calculate reliability versus time.

Reliability versus time was calculated for the disc using stress rate and double torsion data.

## VII. RECOMMENDATIONS

A series of discs should be tested under the conditions documented in this report to experimentally determine reliability versus time. The experimental data so determined could then be compared to the analytical results presented here. This comparison would determine which data base gives the most accurate reliability predictions. The experimental data would also be useful in verifying mathematical models of time dependent failure of structural ceramics and associated computer programs incorporating these models.

## REFERENCES

1. Sage, A. M. and Histed, J. H., "Applications of Silicon Nitride," Powder Metallurgy, No. 8, (1961).
2. Glenny, E. and Taylor, T. A., "Mechanical Strength and Thermal Fatigue Characteristics of Silicon Nitride," Powder Metallurgy, No. 8 (1961).
3. Evans, A. G. and Wiederhorn, S. M., "Crack Propagation and Failure Prediction in Silicon Nitride at Elevated Temperatures," Journal of Materials Science, September, 1974.
4. Siverns, M. J., and Price, A. T., "Crack Growth Under Creep Conditions," Nature, November 21, 1970.
5. Evans, A. G., and Johnson, H., "The Fracture Stress and its Dependence on Slow Crack Growth," Journal of Materials Science, No. 10, (1975).
6. Evans, A. G., "High Temperature Slow Crack growth in Ceramic Materials," Ceramics for High Performance Applications, Ed. John J. Burke, Alvin E. Gorum, and R. Nathan Katz, Chesnut Hill, Massachusetts, Brook Hill, 1974.
7. Williams, D. P., and Evans, A. G., "Simple Method for Studying Slow Crack Growth," Journal of Testing and Evaluation, July, 1973.
8. Charles, R. J., "Dynamic Fatigue of Glass," Journal of Applied Physics, December, 1978.
9. Trantina, G. G., "Strength and Life Prediction for Hot-Pressed Silicon Nitride," Journal of the American Ceramic Society, August, 1979.
10. Quinn, G. D., Characterization of Turbine Ceramics After Long-Term Environmental Exposure, U.S. Department of Energy, April, 1980.

11. DeBell, G. C., and Swank, L. R., Testing of Ceramic Rotors Hot Spin Test Rig and Rotor Preparation, A.S.M.E. paper 80-GT-144, 1980.
12. Paluszny, A. and Nicholls, P. F., "Predicting Time-Dependent Reliability of Ceramic Rotors," Ceramics for High Performance Applications-II. Ed. John J. Burke, Edward N. Lenoc, and R. Nathan Katz, Chesnut Hill, Massachusetts, Brook Hill, 1978.
13. Weibull, W., "A Statistical Theory of the Strength of Materials," Proceedings of the Royal Swedish Institute for Engineering Research, Stockholm, 1939.
14. Vardar, O. and Finnie, I., "An Analysis of the Brazilian Disc Fracture Test Using the Weibull Probabilistic Treatment of Brittle Strength," International Journal of Fracture, June, 1979.
15. Jeryan, R. A., "Use of Statistics in Ceramic Design and Evaluation," Ceramics for High Performance Applications-II, Ed. John J. Burke, Edward N. Lenoe, and R. Nathan Katz, Chesnut Hill, Massachusetts, Brook Hill, 1977.
16. Charles, R. J., "Dynamic Fatigue of Glass," Journal of Applied Physics, December, 1958.
17. McLean, A. F. and Secord, J. R., "Brittle Materials Design, High Temperature Gas Turbine," AMMRC TR 79-12, Interim Report, May, 1979.
18. McLean, A. F. and Fisher, E. A., "Brittle Materials Design, High Temperature Gas Turbine," AMMRC TR 81-14, Final Report, March, 1981.
19. Annis, C. G. and Cargill, J. S., "Modified Double Torsion Method for Measuring Crack Velocity in NC-132," Fracture Mechanics of Ceramics, Volume 4. Ed. R. C. Brandt, D. P. H. Hasselman, and F. F. Lange, New York: Plenum Press, 1977.

20. Govila, R. K., "Material Parameters for Life Prediction in Ceramics," Ceramics for High Performance Applications-III. To be published.
21. Larsen, D. C., Property Screening and Evaluation of Ceramic Turbine Engine Materials, Chicago, ITT Research Institute, 1979.
22. Smith, F. W., Emery, A. F., and Kobayashi, A. S. "Stress Intensity Factors for Penny Shaped Cracks," Journal of Applied Mechanics, December, 1967.
23. Govila, R. K., Methodology for Ceramic Life Prediction and Related Proof testing, U. S. Department of Energy, 1978.
24. Tighe, N. J., "The Structure of Slow Crack Interfaces in Silicon Nitride," Journal of Material Science, 13 (1978).
25. Evans, A. G., "High Temperature Slow Crack Growth in Ceramic Materials," Ceramics for High Performance Applications, Ed. John J. Burke, Alvin E. Gorum, and R. Nathan Katz, Chesnut Hill, Massachusetts, Brook Hill, 1974.
26. Chen, E. P. and Hasselman, D. P. H., "Comparison of the High Temperature Thermal Fatigue Resistance of Hot-pressed Silicon Nitride and Silicon Carbide," Journal of the American Ceramic Society, November-December, 1976.

## Appendix A

### Calculation of Constant "B"

The calculation of time dependent reliabilities is based on the power relation of crack velocity as a function of stress intensity factor.

$$V = AK_I^n \quad A-1$$

The values of A and n are determined experimentally, so a literature search was conducted to find published values to utilize for design and analysis. Table III gives the experimental values that were found. The experimental values were published in graphical or numerical form and the manner of presentation is shown on the table. In the cases of graphical publication the numerical values were found by taking values of velocity, "V", and stress intensity factor, "K<sub>I</sub>", from the graph and substituting into Eqn. A-1. It should be noted that considerable error in the determination of A and n may result from this procedure. Cargill and Annis published their results graphically; however, they furnished the values of A and n determined by least squares fitting of their data. The A and n values of Annis and Cargill<sup>(19)</sup> and Govila<sup>(20)</sup> were used in this program.

The values of A and n available are published for 930°C, 1200°C, and 1300°C. Reliability calculation requires values for A and n at the centroidal temperature of each finite element of the finite element grid shown in Fig. 2. To obtain the required values, linear interpolation was used.

The critical stress intensity factor for the material is an important parameter when double torsion data is used to calculate time dependent reliability. Larsen<sup>(21)</sup> presented graphical data for hot pressed silicon nitride and the numerical values used are shown in Table IV. Also required for the use of double torsion data is an assumption about the shape of the flaw, so that the stress intensity factor coefficient may be determined. For this program the flaws were assumed to be penny shaped internal flow with a stress intensity factor coefficient<sup>(22)</sup> of  $2/\sqrt{\pi}$ .

As shown in Fig. 9 the value of "B" must be computed before reliability versus time can be calculated and the following equations show the evaluation of "B" at 1200°C with the required material and geometric constants and their sources.

	<u>Reference</u>
n = 27.4	19
A = $1.58 \times 10^{-23} \frac{\text{m}}{\text{sec}} \frac{1}{(\text{MPa } \sqrt{\text{m}})^n}$	19
K <sub>IC</sub> = 7.2 MPa√m	21
Y = $2/\sqrt{\pi}$	22

$$B = \frac{2}{(n-2)Y^2 AK_{IC}^{n-2}}$$

$$B = \frac{2}{(27.4-2) \left(\frac{2}{\sqrt{\pi}}\right)^2 1.58 \times 10^{-23} \times (7.2)^{27.4-2}} \times \frac{\text{hr.}}{3600 \text{ sec}}$$

$$B = 0.000182 \text{ MPa}^2 \text{ - hr.}$$

An alternate data base to use for predicting time dependent failure is stress rate data. The NC-132 stress rate data is given in Table V<sup>(23)</sup>. Reference 23 gives data for several stress rates, but the lowest available stress rate and corresponding fracture strength was chosen on the assumption that slow stress rate result was most applicable for predicting stress rupture results. As shown on Fig. 10 the value of "B" must be evaluated before reliability versus time can be calculated and the following equations show a typical calculation.

Temperature = 1204°C

		<u>Reference</u>
n	= 19.9	(23)
$\sigma_f$	= 485 MPa	(23)
$\dot{\sigma}$	= 0.8 MPa/min.	(23)

$$B = \frac{\sigma_f^3}{\dot{\sigma}(n+1)}$$

$$B = \frac{(485)^3}{0.8 \times (19.9+1)} \times \frac{\text{hr.}}{60 \text{ min.}}$$

$$B = 113720 \text{ MPa}^2 \cdot \text{hr.}$$

## APPENDIX B NOMENCLATURE

- A Premultiplier in crack velocity equation, meter/second  $(\text{MPa}\cdot\text{m})^n$ .
- B Constant in reliability versus time equation,  $\text{MPa}^2\text{-hr}$ .
- i ith value of test in a set of tests.
- $K_I$  Stress intensity  $\text{MPa}\sqrt{\text{m}}$ .
- $K_{IC}$  Critical stress intensity, a material parameter,  $\text{MPa}\sqrt{\text{m}}$ .
- n Crack velocity exponent.
- N Number of tests in a set.
- m Weibull modulus.
- $\text{MOR}_0$  Characteristic modulus of rupture, MPa
- R Reliability as a function of time
- $R_{ff}$  Fast fracture reliability
- $\sigma$  Stress, MPa.
- $\sigma_0$  Characteristic strength of the structure, MPa.
- $\sigma_f$  Fracture stress, MPa.
- $\dot{\sigma}$  Stress rate,  $\text{MPa}/\text{min}$ .
- $\sigma_0$  Weibull parameter,  $\text{MPa}/(\text{m}^3)^{\frac{1}{m}}$ .
- T Temperature,  $^{\circ}\text{C}$ .
- t Time, hours.
- V Volume,  $\text{m}^3$ .
- V Crack velocity, m/sec.
- Y Stress intensity factor coefficient, non-dimensional.

APPENDIX C  
SIMPLIFICATION OF RELIABILITY VERSUS TIME FORMULA

Reference 12 gives equation 1 for calculating reliability versus time for an element of a structure.

$$R = \exp \left[ - \left[ \left( \ln \left( \frac{1}{R_{ff}} \right) \right)^{\frac{n-2}{m}} + \frac{\sigma^n t}{\sigma_\theta^{n-2} B} \right]^{\frac{m}{n-2}} \right] \quad (1)$$

This appendix shows the algebra required to simplify Equation 1 to Equation 2.

$$R = R_{ff} \left( 1 + \frac{\sigma^2 t}{B} \right)^{\frac{m}{n-2}} \quad (2)$$

The nomenclature is given in Appendix B.

First use Equation 3 which is the fast fracture reliability of any element.

$$R_{ff} = e^{-\left(\frac{\sigma}{\sigma_\theta}\right)^m} \quad (3)$$

This can be rearranged to give Equation 4.

$$\frac{\sigma}{\sigma_\theta} = \left( \ln \left( \frac{1}{R_{ff}} \right) \right)^{\frac{1}{m}} \quad (4)$$

Now one group of terms in Equation 1 can be written as Equation 5.

$$\frac{\sigma^n t}{\sigma_\theta^{n-2} B} = \left( \frac{\sigma}{\sigma_\theta} \right)^{n-2} \frac{\sigma^2 t}{B} \quad (5)$$

Substitute Equation 4 into Equation 5 to yield Equation 6.

$$\frac{\sigma^n t}{\sigma_\theta^{n-2} B} = \left( \ln \left( \frac{1}{R_{ff}} \right) \right)^{\frac{n-2}{m}} \frac{\sigma^2 t}{B} \quad (6)$$

Appendix C continued

Now use Equation 6 to write Equation 1 as Equation 7.

$$R = \exp \left[ - \left[ \left( \ln \left( \frac{1}{R_{ff}} \right) \right)^{\frac{n-2}{m}} + \left( \ln \left( \frac{1}{R_{ff}} \right) \right)^{\frac{n-2}{m}} \frac{\sigma^2 t}{B} \right]^{\frac{m}{n-2}} \right] \quad (7)$$

Factoring out the  $R_{ff}$  term, Equation 7 becomes Equation 8.

$$R = \exp \left[ - \left[ \left( \ln \frac{1}{R_{ff}} \right)^{\frac{n-2}{m}} \times \left( 1 + \frac{\sigma^2 t}{B} \right) \right]^{\frac{m}{n-2}} \right] \quad (8)$$

Using the laws of exponents, Equation 8 becomes:

$$R = \exp \left[ - \left[ \left( \ln \left( \frac{1}{R_{ff}} \right) \right) \left( 1 + \frac{\sigma^2 t}{B} \right)^{\frac{m}{n-2}} \right] \right] \quad (9)$$

Using the laws of logarithms, Equation 9 becomes:

$$R = \exp \left[ \ln R_{ff} \left( 1 + \frac{\sigma^2 t}{B} \right)^{\frac{m}{n-2}} \right] \quad (10)$$

From the laws of exponents, using  $a^{xy} = (a^x)^y$ , and from the laws of logarithms  $e^{\ln b} = b$ , Equation 10 becomes:

$$R = R_{ff} \left( 1 + \frac{\sigma^2 t}{B} \right)^{\frac{m}{n-2}} \quad (11)$$

Equation 11 simplifies the computation of reliabilities considerably from the use of Equation 1. Also, it simplifies the understanding of how each parameter  $R_{ff}$ ,  $\sigma$ ,  $B$ ,  $t$ ,  $m$ , and  $n$  affect the reliabilities calculated from Equation 1.

TABLE I  
Thermal Properties

	Temperature °F	Thermal Conductivity $\frac{\text{Btu}}{\text{hr ft } ^\circ\text{F}}$	Specific Heat $\text{Btu/lb m}^{-1} ^\circ\text{F}$
Spin Disc and Ceramic	70.	17.	.18
Curvic Spacer Material	500.	15.	.23
Hot Pressed Silicon Nitride	1000.	13.	.26
Density = 3.18 gm/cm <sup>3</sup>	1500.	11.	.29
	2000.	9.2	.33
	2500.	8.0	.32
Nut Material	0.	6.0	.10
Inconel X-750	3000.	20.5	.18
Density = 8.30 gm/cm <sup>3</sup>			
Tie Bolt Material	0.	6.0	.10
Inconel X-718	3000.	21.8	.10
Density = 8.19 gm/cm <sup>3</sup>			
Compression Member	0.	6.5	.11
Material	3000.	25.2	.11
A-286			
Density = 7.91 gm/cm <sup>3</sup>			
Shaft Material	0.	21.7	.11
AMS 6265	3000.	21.7	.11
Density = 7.83 gm/cm <sup>3</sup>			
Curvic Material	70.	3.99	.18
	500.	3.87	.23
Density = 3.18 gm/cm <sup>3</sup>	1000.	3.72	.26
	1500.	3.54	.29
	2000.	3.33	.33
	2500.	3.16	.32

Air	Temperature	Thermal Conductivity $\frac{\text{Btu}}{\text{hr ft } ^\circ\text{F}}$	Specific Heat $\frac{\text{Btu}}{\text{lbm}}$	Density $\frac{\text{lbm}}{\text{ft}^3}$
	0	.013	.239	.0863
	100	.015	.240	.0680
	500	.023	.247	.0392
	800	.028	.256	.0299
	1000	.032	.262	.0258
	1500	.040	.276	.0192
	2000	.047	.286	.0153
	2500	.051	.292	.0127
	3000	.054	.297	.0108

TABLE II

## Elastic Properties

NC-132 Hot Pressed Silicon Nitride	Temperature	Young's Modulus	Poisson's Ratio	Shear Modulus	Coefficient of Thermal Expansion in/in/ <sup>o</sup> F
Density = 3.18 gm/cm <sup>3</sup>	<sup>o</sup> F	x10 <sup>6</sup> psi		x10 <sup>6</sup> psi	x10 <sup>-6</sup>
	78	41.9	.219	17.1	.74
	500	41.9	.203	17.5	.97
	1000	41.8	.190	17.5	1.32
	1500	40.6	.189	17.1	1.53
	2000	38.7	.194	16.1	1.68
	2500	35.4	.194	14.3	1.82

TABLE III

## Crack Velocity Parameters

Material	Temper- ature °C	Crack Velocity Exponent		Reference	Form of Data Presentation
	A	n			
HPSN NC-132	930	$6.18 \times 10^{-56}$	74.7	19	Graphical
HPSN NC-132	1200	$1.58 \times 10^{-23}$	27.4	19	Graphical
HPSN NC-132	1300	$4.3 \times 10^{-9}$	5.6	20	Numerical
HPSN NC-132	1350	$7.9 \times 10^{-9}$	5.6	20	Numerical
HPSN NC-132	1400	$1 \times 10^{-7}$	5.25	20	Numerical
HPSN NC-132	1200	$1.21 \times 10^{-31}$	35.4	24	Graphical
HPSN NC-132	1400	$9 \times 10^{-8}$	5.8	24	Graphical
HPSN HS-130	1250	$1.41 \times 10^{-14}$	10.5	25	Graphical
HPSN HS-130	1300	$9.31 \times 10^{-14}$	11.5	25	Graphical
HPSN HS-130	1350	$9.83 \times 10^{-13}$	10.2	25	Graphical
HPSN HS-130	1400	$3.05 \times 10^{-12}$	10.6	25	Graphical
HPSN HS-130	1200	$2.56 \times 10^{-59}$	73.3	25	Graphical
HPSN HS-130	1400	$8.22 \times 10^{-8}$	4.93	25	Graphical
HPSN	1000 to 1400	$5 \times 10^{-14}$	6	26	Numerical

TABLE IV

Critical Stress Intensity Factor

Temperature	Stress Intensity Factor
°C	MPa $\sqrt{m}$
18	5.
930	5.
1200	7.2
1300	11.0

Reference 21

TABLE V

STRESS RATE DATA OF  
NORTON NC-132 HPSN

<u>Temperature</u> <u>°C</u>	<u>Characteristic</u>		<u>Stress</u>	<u>Number of</u> <u>Samples</u>
	<u>MOR</u> <u>MPa</u>	<u>Weibull</u> <u>Modulus</u>	<u>Rate</u> <u>MPa/min.</u>	
21	787.	6.5	1870.0	30
704	730.	6.0	1.8	5
871	818.	8.5	1.8	5
1038	666.	9.9	1.5	5
1204	485.	8.0	.8	5
1371	313.	11.2	91.0	15

Reference 23

## DISTRIBUTION LIST

No. of Copies	To	No. of Copies	To
1	Office of the Under Secretary of Defense for Research and Engineering, The Pentagon, Washington, DC 20301	1	Commander, U.S. Army Test and Evaluation Command, Aberdeen Proving Ground, MD 21005
1	ATTN: Mr. J. Perish	1	ATTN: DRSTE-ME
1	Dr. G. Gamota		
12	Commander, Defense Technical Information Center, Cameron Station, Building 5, 5010 Duke Street, Alexandria, VA 22314	1	Commander, U.S. Army Foreign Science and Technology Center, 220 7th Street, N.E., Charlottesville, VA 22901
1	National Technical Information Service, 5285 Port Royal Road, Springfield, VA 22161	1	ATTN: Military Tech, Mr. W. Marley
	Director, Defense Advanced Research Projects Agency, 1400 Wilson Boulevard, Arlington, VA 22209	1	Commander, Watervliet Arsenal, Watervliet, NY 12189
1	ATTN: Dr. A. Bement	1	ATTN: Dr. T. Davidson
1	Dr. Van Reuth		
1	MAJ Harry Winsor	1	Director, Eustis Directorate, U.S. Army Mobility Research and Development Laboratory, Fort Eustis, VA 23604
	Battelle Columbus Laboratories, Metals and Ceramics Information Center, 505 King Avenue, Columbus, OH 43201	1	ATTN: Mr. J. Robinson, DAVDL-E-MOS (A/R&D COM)
1	ATTN: Mr. Winston Duckworth	1	Mr. C. Walker
1	Dr. D. Niesz		
1	Dr. R. Wills	1	Chief of Naval Research, Arlington, VA 22217
	Deputy Chief of Staff, Research, Development, and Acquisition, Headquarters, Department of the Army, Washington, DC 20301	1	ATTN: Code 471
1	ATTN: DAMA-AP2	1	Dr. A. Diness
1	DAMA-CSS, Dr. J. Bryant	1	Dr. R. Pohanka
	Commander, U.S. Army Medical Research and Development Command, Fort Detrick, Frederick, MD 21701	1	Naval Research Laboratory, Washington, DC 20375
1	ATTN: SGRD-SI, Mr. Lawrence L. Ware, Jr.	1	ATTN: Dr. J. M. Krafft - Code 5830
	Commander, Army Research Office, P.O. Box 12211, Research Triangle Park, NC 27709	1	Mr. R. Rice
1	ATTN: Information Processing Office		
1	Dr. G. Mayer	1	Headquarters, Naval Air Systems Command, Washington, DC 20360
1	Dr. J. Hurt	1	ATTN: Code 5203
	Commander, U.S. Army Materiel Development and Readiness Command, 5001 Eisenhower Avenue, Alexandria, VA 22333	1	Code MAT-042M
1	ATTN: DRCDMD-ST	1	Mr. I. Macklin
1	DRCLDC		
	Commander, Harry Diamond Laboratories, 2800 Powder Mill Road, Adelphi, MD 20783	1	Commander, Naval Weapons Center, China Lake, CA 93555
1	ATTN: Mr. A. Benderly	1	ATTN: Mr. F. Markarian
1	Technical Information Office		
1	DELHD-RAE	1	Commander, U.S. Air Force of Scientific Research, Building 410, Bolling Air Force Base, Washington, DC 20332
	Commander, U.S. Army Missile Command, Redstone Arsenal, AL 35809	1	ATTN: MAJ W. Simmons
1	ATTN: Mr. P. Ormsby		
1	Technical Library	1	Commander, U.S. Air Force Wright Aeronautical Laboratories, Wright-Patterson Air Force Base, OH 45433
	Commander, U.S. Army Aviation Research and Development Command, 4300 Goodfellow Boulevard, St. Louis, MO 63120	1	ATTN: AFWAL/MLLM, Dr. N. Tallan
1	ATTN: DRDAV-EGX	1	AFWAL/MLLM, Dr. H. Graham
1	DRDAV-QE	1	AFWAL/MLLM, Dr. R. Ruh
	Commander, U.S. Army Tank-Automotive Command, Warren, MI 48090	1	AFWAL/MLLM, Dr. A. Katz
1	ATTN: Dr. W. Bryzik	1	AFWAL/MLLM, Mr. K. S. Mazdiyazni
1	Mr. E. Hamperian	1	Aero Propulsion Labs, Mr. R. Marsh
1	D. Rose		
1	DRSTA-RKA	1	National Aeronautics and Space Administration, Washington, DC 20546
1	DRSTA-UL, Technical Library	1	ATTN: Mr. G. C. Deutsch - Code RW
1	DRSTA-R	1	Mr. J. Gangler
	Commander, U.S. Army Armament Research and Development Command, Dover, NJ 07801	1	AFSS-AD, Office of Scientific and Technical Information
1	ATTN: Dr. G. Vezzoli		
1	Technical Library	1	National Aeronautics and Space Administration, Lewis Research Center, 21000 Brookpark Road, Cleveland, OH 44135
	Commander, U.S. Army Armament Materiel Readiness Command, Rock Island, IL 61299	1	ATTN: J. Accario, USAMRDL
1	ATTN: Technical Library	1	Mr. H. B. Probst, MS 49-1
	Commander, Aberdeen Proving Ground, MD 21005	1	Dr. R. Ashbrook
1	ATTN: DRDAR-CLB-PS, Mr. J. Vervier	1	Dr. S. Dutta
	Commander, U.S. Army Mobility Equipment Research and Development Command, Fort Belvoir, VA 22060	1	Mr. S. Grisaffe
1	ATTN: DRCME-EM, Mr. W. McGovern		
1	DRCME-V, Mr. E. York	1	National Aeronautics and Space Administration, Langley Research Center, Center, Hampton, VA 23665
	Director, U.S. Army Ballistic Research Laboratory, Aberdeen Proving Ground, MD 21005	1	ATTN: Mr. J. Buckley, Mail Stop 367
1	ATTN: DRDAR-TSB-S (STINFO)		
		1	Department of Energy, Division of Transportation, 20 Massachusetts Avenue, N.W., Washington, DC 20545
		1	ATTN: Mr. George Thur (TEC)
		1	Mr. Robert Schulz (TEC)
		1	Mr. John Neal (CLHRT)
		1	Mr. Steve Wander (Fossil Fuels)
		1	Department of Transportation, 400 Seventh Street, S.W., Washington, DC 20590
		1	ATTN: Mr. M. Lauriente
		1	National Bureau of Standards, Washington, DC 20234
		1	ATTN: Dr. S. Wiederhorn
		1	National Research Council, National Materials Advisory Board, 2101 Constitution Avenue, Washington, DC 20418
		1	ATTN: D. Groves
		1	R. M. Scriggs
		1	National Science Foundation, Washington, DC 20550
		1	ATTN: B. A. Wilcox

No. of Copies	To	No. of Copies	To
1	Admiralty Materials Technology Establishment, Polle, Dorset BH16 6JU, UK	1	Kawecki Berylic Industries, Inc., P.O. Box 1462, Reading, PA 19603
1	ATTN: Dr. D. Godfrey	1	ATTN: Mr. R. J. Longenecker
1	ATTN: Dr. M. Lindley		
1	AiResearch Manufacturing Company, AiResearch Casting Company, 2525 West 190th Street, Torrance, CA 90505	1	Martin Marietta Laboratories, 1450 South Rolling Road, Baltimore, MD 21227
1	ATTN: Mr. K. Styhr	1	ATTN: Dr. J. Venables
1	AiResearch Manufacturing Company, Materials Engineering Dept., 111 South 34th Street, P.O. Box 5117, Phoenix, AZ 85010	1	Massachusetts Institute of Technology, Department of Metallurgy and Materials Science, Cambridge, MA 02139
1	ATTN: Mr. D. W. Richerson, MS 93-393/493-44	1	ATTN: Prof. R. L. Coble
		1	Prof. h. K. Bowen
		1	Prof. W. D. Kingery
1	AVCO Corporation, Applied Technology Division, Lowell Industrial Park, Lowell, MA 01887		
1	ATTN: Dr. T. Vasilos		
1	Carborundum Company, Research and Development Division, P.O. Box 1054, Niagara Falls, NY 14302	1	Midwest Research Institute, 425 Volker Boulevard, Kansas City, MO 64110
1	ATTN: Dr. J. A. Coppola	1	ATTN: Mr. Gordon W. Gross, Head, Physics Station
1	Case Western Reserve University, Department of Metallurgy, Cleveland, OH 44106	1	Norton Company, Worcester, MA 01606
1	ATTN: Prof. A. H. Heuer	1	ATTN: Dr. N. Ault
		1	Dr. M. L. Torti
1	Cummins Engine Company, Columbus, IN 47201	1	Pennsylvania State University, Materials Research Laboratory, Materials Science Department, University Park, PA 16802
1	ATTN: Mr. R. Kano	1	ATTN: Prof. R. E. Tressler
		1	Prof. R. Bradt
		1	Prof. V. S. Stubican
1	Deposits and Composites, Inc., 1821 Michael Faraday Drive, Reston, VA 22090	1	RIAS, Division of the Martin Company, Baltimore, MD 21203
1	ATTN: Mr. R. E. Engdahl	1	ATTN: Dr. A. R. C. Westwood
1	Electric Power Research Institute, P.O. Box 10412, 3412 Hillview Avenue, Palo Alto, CA 94304	1	Stanford Research International, 333 Ravenswood Avenue, Menlo Park, CA 94025
1	ATTN: Dr. A. Cohn	1	ATTN: Dr. P. Jorgensen
		1	Dr. D. Rowcliffe
1	European Research Office, 223 Old Marylebone Road, London, NW1 - Sthe, England		
1	ATTN: Dr. R. Quattrone	1	State University of New York at Stony Brook, Department of Materials Science, Long Island, NY 11790
1	LT COL James Kennedy	1	ATTN: Prof. Franklin F. Y. Wang
1	Ford Motor Company, Turbine Research Department, 20000 Rotunda Drive, Dearborn, MI 48121	1	United Technologies Research Center, East Hartford, CT 06108
1	ATTN: Mr. A. F. McLéan	1	ATTN: Dr. J. Brennan
1	Mr. E. A. Fisher	1	Dr. F. Galasso
1	Mr. J. A. Mangels		
1	Mr. R. Govila		
1	General Electric Company, Research and Development Center, Box 8, Schenectady, NY 12345	1	University of California, Lawrence Livermore Laboratory, P.O. Box 808, Livermore, CA 94550
1	ATTN: Dr. R. J. Charles	1	ATTN: Dr. C. F. Cline
1	Dr. C. D. Greskovich		
1	Dr. S. Prochazka	1	University of Florida, Department of Materials Science and Engineering, Gainesville, FL 32601
1	General Motors Corporation, AC Spark Plug Division, Flint, MI 48556	1	ATTN: Dr. L. hench
1	ATTN: Dr. M. Berg	1	University of Newcastle Upon Tyne, Department of Metallurgy and Engineering Materials, Newcastle Upon Tyne, NE1 7 RU, England
1	Georgia Institute of Technology, EES, Atlanta, GA 30332	1	ATTN: Prof. K. H. Jack
1	ATTN: Mr. J. D. Walton	1	University of Washington, Ceramic Engineering Division, FB-10, Seattle, WA 98195
1	GTE Laboratories, Waltham Research Center, 40 Sylvan Road, Waltham, MA 02154	1	ATTN: Prof. James I. Mueller
1	ATTN: Dr. C. Quackenbush	1	Westinghouse Electric Corporation, Research Laboratories, Pittsburgh, PA 15235
1	Dr. W. H. Rhodes	1	ATTN: Dr. R. J. Bratton
1	IIT Research Institute, 10 West 35th Street, Chicago, IL 60616		
1	ATTN: Mr. S. Bortz, Director, Ceramics Research	2	Director, Army Materials and Mechanics Research Center, Watertown, MA 02172
		1	ATTN: DRXMR-PL
		1	DRXMR-PR
		1	DRXMR-K
		1	DRXMR-FD
		10	DRXMR-SM, Dr. E. Lenoé
1	Institut für Werkstoff-Forschung, DFVLR, 505 Porz-Wahn, Linder Höhe, Germany		
1	ATTN: Dr. W. Bunk		
1	International Harvester, Solar Division, 2200 Pacific Highway, P.O. Box 80966, San Diego, CA 92138		
1	ATTN: Dr. A. Metcalfe		
1	Ms. M. E. Gulden		

AD UNCLASSIFIED  
UNLIMITED DISTRIBUTION

Army Materials and Mechanics Research Center,  
Watertown, Massachusetts 02172  
CERAMIC LIFE PREDICTION METHODOLOGY -  
HOT SPIN DISC LIFE PROGRAM -  
R. R. Baker, L. R. Sank, and J. C. Caverly

Key Words

Brittle design  
Ceramics  
High temperature  
Materials  
Silicon nitride  
Silicon carbide  
Mechanical properties

AD UNCLASSIFIED  
UNLIMITED DISTRIBUTION

Army Materials and Mechanics Research Center,  
Watertown, Massachusetts 02172  
CERAMIC LIFE PREDICTION METHODOLOGY -  
HOT SPIN DISC LIFE PROGRAM -  
R. R. Baker, L. R. Sank, and J. C. Caverly

Key Words

Brittle design  
Ceramics  
High temperature  
Materials  
Silicon nitride  
Silicon carbide  
Mechanical properties

A rotating disc was designed to fail due to time-dependent mechanisms. Several discs were fabricated and a previously existing test rig was developed to test the discs at the design conditions. A successful calibration test was conducted at the design conditions of 2300°F rim temperature and 50,000 rpm. The disc failed after eight and one-half hours of steady-state testing indicating that the design was successful, since the failure was due to a time-dependent mechanism.

A rotating disc was designed to fail due to time-dependent mechanisms. Several discs were fabricated and a previously existing test rig was developed to test the discs at the design conditions. A successful calibration test was conducted at the design conditions of 2300°F rim temperature and 50,000 rpm. The disc failed after eight and one-half hours of steady-state testing indicating that the design was successful, since the failure was due to a time-dependent mechanism.

AD UNCLASSIFIED  
UNLIMITED DISTRIBUTION

Army Materials and Mechanics Research Center,  
Watertown, Massachusetts 02172  
CERAMIC LIFE PREDICTION METHODOLOGY -  
HOT SPIN DISC LIFE PROGRAM -  
R. R. Baker, L. R. Sank, and J. C. Caverly

Key Words

Brittle design  
Ceramics  
High temperature  
Materials  
Silicon nitride  
Silicon carbide  
Mechanical properties

AD UNCLASSIFIED  
UNLIMITED DISTRIBUTION

Army Materials and Mechanics Research Center,  
Watertown, Massachusetts 02172  
CERAMIC LIFE PREDICTION METHODOLOGY -  
HOT SPIN DISC LIFE PROGRAM -  
R. R. Baker, L. R. Sank, and J. C. Caverly

Key Words

Brittle design  
Ceramics  
High temperature  
Materials  
Silicon nitride  
Silicon carbide  
Mechanical properties

A rotating disc was designed to fail due to time-dependent mechanisms. Several discs were fabricated and a previously existing test rig was developed to test the discs at the design conditions. A successful calibration test was conducted at the design conditions of 2300°F rim temperature and 50,000 rpm. The disc failed after eight and one-half hours of steady-state testing indicating that the design was successful, since the failure was due to a time-dependent mechanism.

A rotating disc was designed to fail due to time-dependent mechanisms. Several discs were fabricated and a previously existing test rig was developed to test the discs at the design conditions. A successful calibration test was conducted at the design conditions of 2300°F rim temperature and 50,000 rpm. The disc failed after eight and one-half hours of steady-state testing indicating that the design was successful, since the failure was due to a time-dependent mechanism.

